

ROGUE WAVES IN ULTRACOLD BOSONIC SEAS

E. G. CHARALAMPIDIS^{1,*}, J. CUEVAS-MARAVAR², D. J. FRANTZESKAKIS³,
P. G. KEVREKIDIS¹

¹Department of Mathematics and Statistics, University of Massachusetts Amherst,
Amherst, MA 01003-4515, USA

²Grupo de Física No Lineal, Departamento de Física Aplicada I, Universidad de Sevilla, Escuela
Politécnica Superior, C/ Virgen de África, 7, 41011-Sevilla, Spain
Instituto de Matemáticas de la Universidad de Sevilla (IMUS), Edificio Celestino Mutis, Avda. Reina
Mercedes s/n, 41012-Sevilla, Spain

³Department of Physics, National and Kapodistrian University of Athens, Panepistimiopolis,
Zografos, Athens 15784, Greece

*Corresponding author, Email: charalamp@math.umass.edu

Received June 26, 2017

Abstract. In this work, we numerically consider the initial value problem for nonlinear Schrödinger (NLS)-type models arising in the physics of ultracold bosonic gases, with generic Gaussian wavepacket initial data. The corresponding Gaussian's width and, wherever relevant, also its amplitude serve as control parameters. First, we explore the one-dimensional, standard NLS equation with general power law nonlinearity, in which large amplitude excitations *reminiscent* of Peregrine solitons or regular solitons appear to form, as the width of the relevant Gaussian is varied. Furthermore, the variation of the nonlinearity exponent aims at exploring the interplay between rogue waves and the emergence of collapse. The robustness of the main features to noise in the initial data is also confirmed. To better connect our study with the physics of atomic condensates, and explore the role of dimensionality effects, we also consider the non-polynomial Schrödinger equation, as well as the full three-dimensional NLS equation, and examine the degree to which relevant considerations generalize.

Key words: rogue waves, ultracold bosonic gases.

1. MOTIVATION AND BACKGROUND

Over the past decade, the study of extreme wave events and patterns, known as rogue or freak waves, has constituted one of the focal points of both intense theoretical analysis and a wide range of physical applications [1–3]. In particular, such structures have emerged in a diverse host of experiments carried out in a broad array of physical systems including – but not limited to – nonlinear optics [4–8], mode-locked lasers [9], superfluid helium [10], hydrodynamics [11–13], Faraday surface ripples [14], parametrically driven capillary waves [15], and plasmas [16]. In addition, an abundance of theoretical investigations followed the seminal works of Peregrine [17], Kuznetsov [18], Ma [19], and Akhmediev [20], as well as Dysthe and

Trulsen [21], which examined rational solutions of prototypical dispersive nonlinear systems, such as the nonlinear Schrödinger (NLS) equation. A large part of the considerable volume of theoretical research has by now been summarized in a number of reviews [22–25].

At the same time, the last twenty years have seen a tremendous growth of interest in the study of solitary waves in the realm of ultracold bosonic atom gases and Bose-Einstein condensates (BECs) [26–30], as well as, more recently, damped-driven (open system) siblings, namely exciton-polariton condensates [31]. This is because – especially so at the Hamiltonian atomic setting of ultracold and dilute enough gases – an accurate mean-field description gives rise to the NLS model, typically in the presence of a trap; in this context, the NLS equation is usually referred to as the Gross-Pitaevskii equation (GPE) [26, 27]. Moreover, depending on the type of interatomic interactions (repulsive or attractive), which is controlled by the sign of the s -wave scattering length, a self-defocusing or self-focusing nonlinearity in the equation emerges, leading to a wide array of potentially relevant nonlinear wave structures. Among the ones that have been experimentally verified and intensely theoretically studied, we can classify the one-dimensional (1D) bright [32–34], gap [35], and dark [36] matter-wave solitons; we note here that Faraday wave patterns have also been of interest [37–42]. Higher-dimensional analogues of nonlinear waves, namely vortices [43, 44], in the two-dimensional (2D) setting, as well as vortex lines and vortex rings in the three-dimensional (3D) setting [45], are also particularly interesting and relevant, and accessible to experiments (see the recent book [30] and references therein).

On the other hand, there is a large volume of theoretical work devoted to studies on rogue waves in atomic BECs. Relevant investigations, following the – fundamental in this context – study of Ref. [46], include studies in single-component [47–53], binary mixtures [54–61], as well as three-component and spinor BECs [62–64], in quasi-1D settings. Moreover, rogue waves in higher-dimensional BECs, namely in quasi-2D [65] and 3D [66] nonautonomous settings, were also studied. Nevertheless, intriguingly enough, while attractive atomic BECs are natural candidates to support rogue waves (as they are described by focusing NLS-type models) we are not aware of an effort to produce *experimentally* a rogue wave – *e.g.*, a Peregrine soliton in a condensate of ^7Li or ^{85}Rb atoms. This may structurally have to do with the difficulty of preparing the initial background state leading to such a rogue wave. Nevertheless, it should be pointed out here that recent BEC experiments enjoy a tremendous amount of control and, in that light, our present setting could hopefully ignite further experimental realizations. For instance, the work of [67] demonstrates methods towards creating arbitrary types of potentials, while it is also possible to switch the nature of interatomic interactions and study systematically bright soliton-inducing instabilities and effective (phase dependent) interactions; see, *e.g.*, [68]. We thus ex-

pect that it will be possible to prepare initial wavepackets of the type proposed below, both in atomic, but also in optical realizations of the relevant NLS models.

In the case of the Peregrine soliton, before it “appears out of nowhere” and after it “disappears without a trace” (features often alluded to rogue waves [69, 70]), the background state is an unstable uniform one that naturally leads to instabilities and the formation of patterns (see, *e.g.*, the discussion in Ref. [71] and the recent work [72]). Hence, a natural question to ask is whether these two themes, the rogue wave patterns and the atomic condensate realm, may possess a nontrivial interaction point whereby a suitable initial condition could be utilized to produce a pattern strongly reminiscent, *e.g.*, of a Peregrine soliton. This is our starting point motivating the present study.

More concretely, a brief description of our investigations and presentation of this work is as follows. We focus on a well-defined array of physically realistic numerical experiments in a set of models, relevant to the BEC physics, which are summarized in Sec. 2. Our initial condition has the generic form of a matter wave packet that is supported by attractive BECs [26, 27], namely a Gaussian one, parametrized chiefly by its width (but in some cases, as relevant and as will be seen below, also potentially by its amplitude). When the width of this wavepacket is large, we expect it to self-focus and potentially yield a large amplitude event; the latter will be compared (favorably, as will be illustrated below) to a Peregrine soliton, although connections of the evolution with N -soliton solutions will also be sought.* On the other hand, if the width is small, we expect the pattern to adjust to a solitonic wavepacket. In this way, in some sense, we seek a rogue-wave-to-soliton transition (in Sec. 3) as the width of the wavepacket is varied in the system. This phenomenology constitutes the backbone of our observations herein.

Subsequently, we explore different types of variations to this theme. Initially, we examine the role of noisy perturbations to the initial conditions. Here we see that such perturbations are of progressively more limited role as the width is decreased, but overall importantly they do not destroy the relevant phenomenology. Another dimension of our numerical explorations in the same Section concerns the interplay of the above features with another class of extreme events that are potentially supported by NLS-type models, namely self-focusing and wave collapse. To that effect, we examine also the power-law generalization of the NLS model (where the power of the nonlinearity is characterized by a general exponent), so as to enable the extreme wave formation to co-exist with unstable solitons and stable collapse events. This will be

*It is relevant to point out here that in the present setting the term N -soliton will be used in the spirit of the analysis of the inverse scattering problem, rather than the more “colloquial” sense of a waveform bearing N -isolated single soliton pulses. For clarity, relevant profiles of N -soliton solutions, *e.g.*, for $N = 2$ and $N = 3$ are given in an explicit form, as obtained by the inverse scattering method, in the Appendix of the text.

observed below to potentially lead to strong focusing events even in the case of sub-critical NLS models. In Sec. 4, we broach more concretely the possibility of realizing these observations in a physical system of atomic BECs. To do so, we go beyond the 1D mean-field, NLS-based approximation to a more realistic study of the so-called non-polynomial Schrödinger equation (NPSE); the latter, was introduced some time ago to take into account the effect of the deviation from one-dimensionality on the longitudinal BEC dynamics [73]. Importantly, results obtained in the framework of the NPSE model compare favorably with ones obtained from the full 3D GPE, as well as experimental observations on dark solitons in single-component repulsive BECs [74], dark-bright solitons in binary repulsive BECs [75] and, more recently, on bright solitons in single-component attractive BECs [76]; thus, the NPSE is appreciated to be a considerably improved approximation towards capturing the fully 3D dynamics. For comparison here, we present both the NPSE and the 3D GPE results; these suggest that large amplitude events with the same type of initial data are possible, but at the same time, some of the more “delicate” phenomenology of the original NLS model appears to be lost. Finally, in Sec. 5, we summarize our findings and present some considerations and possibilities for future studies.

2. ANALYTICAL CONSIDERATIONS

2.1. THE ONE-DIMENSIONAL CASE: THE MODELS AND ANALYTICAL SETUP

We start by presenting our 1D models and the analytical setup. To this end, the first model of interest is the 1D NLS equation with a focusing, power-law nonlinearity given by

$$i\partial_t u = -\frac{1}{2}\partial_x^2 u - |u|^{2\delta} u, \quad (1)$$

where $u = u(x, t) \in \mathbb{C}$ and δ determines the nonlinearity power. We will start by exploring the integrable case of $\delta = 1$, and consider the cases with $\delta > 1$ afterwards (see Sec. 3.2 below). Here we should point out that for $\delta = 1$ Eq. (1) reduces to the GPE, with $u(x, t)$ standing for the macroscopic wavefunction of a 1D attractive BEC [29]. In the case of $\delta = 1$ for atomic BECs, perhaps the most physically relevant context to bear in mind is that of a toroidal trap confining tightly the BEC along the azimuthal direction. In such a setting, the BEC is trapped within a large radius ring, effectively emulating a 1D scenario with periodic boundary conditions, as is relevant also in the simulations. This scenario has been discussed earlier, *e.g.*, in Ref. [77], yet a recent reference detailing also the reduction and adimensionalization of the 1D equation can be found in Ref. [78].

Nevertheless, as explained above, an investigation of cases with $\delta \neq 1$, which will be discussed below, is expected to shed light on the interplay of the emergence of extreme events with nonlinearity. This investigation is partly motivated

by the formation of matter-wave bright solitons during the collapse of attractive higher-dimensional BECs (see the experimental work [34] and theoretical results in Ref. [79]): such a collapse may also occur in the supercritical 1D NLS model with $\delta > 1$ [80].

In order to turn to a genuinely 1D (*i.e.*, not in an azimuthal variable) more realistic class of models for atomic BECs, as discussed above, we will also consider the NPSE model. The latter, which is used to describe quasi-1D BECs [73], has the form:

$$i\partial_t u = -\frac{1}{2}\partial_x^2 u + V(x)u + \frac{1 - (3/2)|u|^2}{\sqrt{1 - |u|^2}}u. \quad (2)$$

Here, we will also include the effect of the external potential $V(x)$, assuming the typical harmonic form of $V(x) = \frac{1}{2}\Omega^2 x^2$ with normalized trap strength Ω . The presence of the potential is a common ingredient for experimental realizations in BECs, and given our aim in this work to establish comparisons with experimental ${}^7\text{Li}$ BECs, we naturally include this feature. Note that $\Omega = 0$ corresponds to the case where the trap is absent, while $\Omega = \Omega_0$ with $\Omega_0 = 0.0193$ is a typical value used in experiments (see, *e.g.*, Ref. [76]) [81].

A crucial feature of our exploration is the assumed Gaussian form of our initial wavepacket, namely

$$u(x, t = 0) = \alpha \exp\left(-\frac{x^2}{2\sigma^2}\right), \quad (3)$$

with amplitude α and width σ . Our main focus in what follows will be to consider variations of σ and their corresponding impact on the dynamics. However, in some cases (especially, as concerns the realistic BEC problem), we will also explore variations of α .

It is relevant in this context, and specifically for the integrable NLS case of Eq. (1) (*i.e.*, for $\delta = 1$ therein), to connect our numerical findings below with the analysis of the Zakharov-Shabat eigenvalue problem; notice that the compatibility condition of the latter is the integrable NLS equation [82]. For single lobe, analytic initial data, such as that of Eq. (3), this analysis can be traced to the work of [83, 84]. In the first of these works [83], it is proved that for single lobe, analytic initial data – as is the case (in our main Gaussian example) here – purely N -soliton solutions result. These are associated with imaginary eigenvalues in the Zakharov-Shabat eigenvalue problem. In the second work [84], this analysis is taken one significant step further, by providing an *explicit* condition that relates the number of solitons in the solution (number of imaginary eigenvalues in the Zakharov-Shabat problem) to the L^1 norm of the initial profile. In particular, the number of simple, imaginary eigen-

values in this case is given by:

$$N = \left\lfloor \frac{1}{2} + \frac{1}{\pi} \int_{\mathbb{R}} |u(x,0)| dx \right\rfloor, \quad (4)$$

where the bracket denotes the floor function, which maps a real number to the largest previous or the smallest following integer. In our case, this number is evaluated as $N = \lfloor 0.5 + (2/\pi)^{1/2} \alpha \sigma \rfloor$, based on the initial data of Eq. (3).

The main emphasis of the present study will be on the classification of the resulting pulses obtained numerically into solitons or, potentially, rogue waves; the former, are described by a sech-profile (*i.e.*, the customary bright or fundamental soliton), and the latter by the algebraically decaying Peregrine soliton [17]. Both of these correspond to exact solutions to the NLS equation (1), and we thus briefly mention the functional form of both waveforms utilized herein. The bright soliton at hand is given by:

$$u(x,t) = A \operatorname{sech}[A(x-x_0)] \exp[i(A^2/2)t], \quad (5)$$

with position of the pulse x_0 and amplitude A . In the following, we keep the position of the pulse fixed, thus setting $x_0 = 0$. On the other hand, and as per the rogue wave solutions themselves, we will be utilizing a form of the Peregrine soliton (used, *e.g.*, in Ref. [85]), involving a free parameter P_0 , set by the boundary conditions (*i.e.*, $\lim_{|x| \rightarrow \infty} |u(x,t)|^2 \rightarrow P_0$); this solution is of the form:

$$u(x,t) = \sqrt{P_0} \left[1 - \frac{4(1+2iP_0t)}{1+4P_0x^2+4P_0^2t^2} \right] \exp(iP_0t). \quad (6)$$

In what follows, we will be interested in investigating whether the waveforms found numerically match a soliton or a Peregrine rogue wave pattern. To that effect, we will isolate the above presented structures at $t = 0$ and utilize, respectively A and P_0 as fitting parameters to obtain the “best-fit soliton” or the “best-fit Peregrine” and discuss which fit is most suitable in each case as we vary σ .

2.2. THE THREE-DIMENSIONAL CASE: THE MODEL AND ANALYTICAL SETUP

When generalizing our 1D NPSE considerations to 3D BECs, we will examine the radially symmetric 3D NLS/GP equation, written in cylindrical coordinates, (ρ, x) , as follows:

$$i \frac{\partial \psi}{\partial t} = -\frac{1}{2} \left(\frac{\partial^2 \psi}{\partial \rho^2} + \frac{1}{\rho} \frac{\partial \psi}{\partial \rho} + \frac{\partial^2 \psi}{\partial x^2} \right) + V(\rho, x) \psi - |\psi|^2 \psi, \quad (7)$$

together with the 3D potential

$$V(\rho, x) = \frac{1}{2}(\rho^2 + \Omega^2 x^2). \quad (8)$$

Motivated by the cigar-shaped BEC setup analyzed in Ref. [76], we fix the value of the normalized trap strength to be of $\Omega = \Omega_0 = 0.0193$.

In analogy to Ref. [73], and as far as the initialization of the dynamics is concerned in this case, we employ Gaussian-like initial conditions of the form of

$$\psi(\rho, x, t = 0) = \frac{\exp[-\rho^2/2\eta(x)^2]}{\sqrt{\pi}\eta(x)}\phi(x), \quad (9)$$

with functions $\phi(x)$ and $\eta(x)$ given by

$$\phi(x) = \alpha \exp\left(-\frac{x^2}{2\sigma^2}\right), \quad \eta(x) = (1 - |\phi(x)|^2)^{1/4}, \quad (10)$$

respectively. Note that the function ϕ is purely a Gaussian with amplitude α and width σ , which are again the canonical parameters of variation in what follows.

3. NUMERICAL RESULTS AND DISCUSSION

To advance Eqs. (1) and (2) forward in time, we employ an exponential time-differencing method combined with Fourier spectral collocation in space [86]. However, there exist alternative numerical methods for advancing the GPE forward in time such as the Crank-Nicolson one (and its parallel version); see, *e.g.*, [87–91] for some relevant references.

3.1. THE INTEGRABLE CASE: $\delta = 1$

In this Section we present numerical results on the dynamics of the NLSE (1) for $\delta = 1$, which is initialized by the Gaussian pulse (3) with $\alpha = 1$. We study the underlying initial value problem (IVP) as a function of σ and focus on the interval $\sigma \in [0.3, 30]$; see, also, Ref. [92] for a complete movie of the dynamics. Furthermore, a fitting process is employed in order to optimally identify as well as classify the reported waves into solitons or rogue waves, as relevant. To that effect, the exact and stationary solutions given by Eqs. (5) and (6) will be utilized, with A and P_0 being the optimization parameters as discussed above.

We now present our results, by considering first the rogue wave regime, that is, the interval of σ where the first high-amplitude waveform obtained numerically best fits to a Peregrine soliton. The top and bottom panels of Fig. 1 highlight example cases belonging to this class, with the monitored density $|u(x, t)|^2$ corresponding to $\sigma = 30$ and $\sigma = 20.1$, respectively. In the realm of Eq. (4), the number of solitons N in the respective cases studied herein are $N = 24$ and $N = 16$. It can be discerned from the left panels of the figure, as well as their respective zoom-ins in the middle panels, that the Gaussian pulse tends to focus and is progressively transformed into

a high-peaked wave (in its density), surrounded by two local minima. As the right panels illustrate, the resulting structure can be deemed as faithfully representing (the core of) a Peregrine soliton. Specifically, the densities at times $t = 17.724$ (top) and $t = 12.342$ (bottom) of the respective cases are shown with solid red lines, while the exact ones, coming from the one-parameter family of rogue waves (6), are presented too with solid blue lines, for comparison. These panels suggest a fairly good agreement between the two. We note in passing that the π phase-jump as has also been reported in Refs. [93, 94] (for such initial data therein) is ubiquitous in our findings too as per the ‘‘Peregrine-like’’ structures at hand. In particular, the top and bottom panels of Fig. 2 present the phase dynamics slightly before and after the emergence of the respective ‘‘Peregrine-like’’ structures of Fig. 1. The expected phase jump can be clearly discerned in these panels.

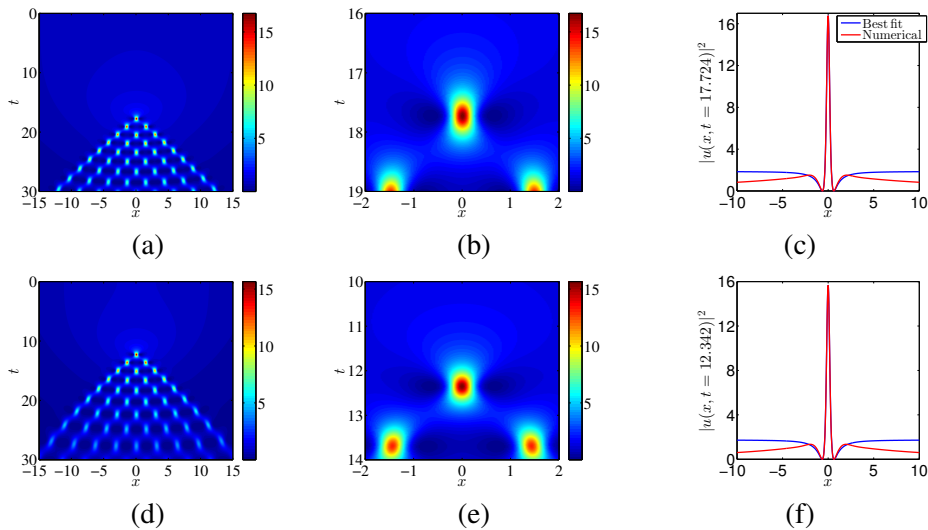


Fig. 1 – (Color online) Summary of results corresponding to $\sigma = 30$ (top row) and $\sigma = 20.1$ (bottom row). Spatiotemporal evolution of the density $|u|^2$ and its zoom-ins are presented in the left and middle columns, respectively. Note that time t increases from top to bottom along the vertical axes in these panels. Spatial distribution of the density at $t = 17.724$ and $t = 12.342$ (at which the first peak is formed) is depicted by solid red lines in the right column. The densities originated from the best-fit Peregrine for this extreme event are plotted too by solid blue lines, for comparison.

At this point, some clarification is necessary: the Peregrine structure ‘‘lives’’ on top of an infinite background while our Gaussian has a decaying tail. Hence, the fitting process is only considered in an interval around the core, as is also evident by the disparity of the tails of the two structures. Nevertheless, these Peregrine structures are the natural candidates that we consider within the class of NLS models as potential rogue wave patterns in this work (see, *e.g.*, Fig. 2 as per the expected

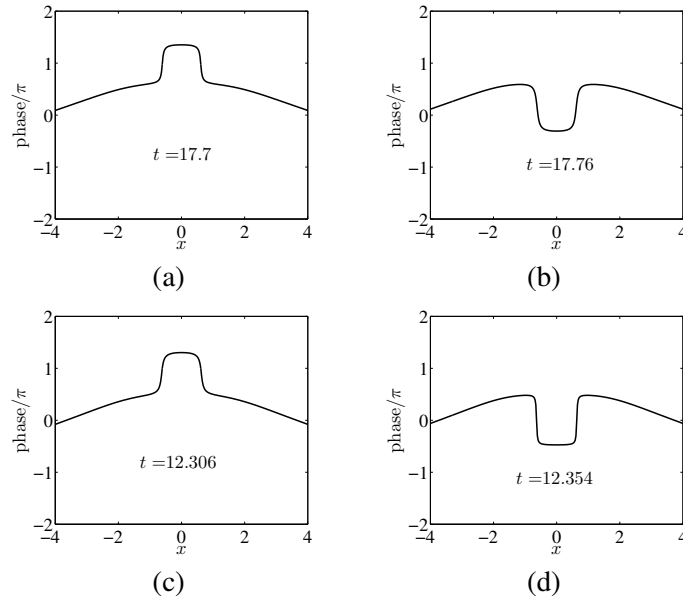


Fig. 2 – Phase dynamics slightly *before* (left column) and *after* (right column) the emergence of the “Peregrine-like” structures of Fig. 1. First and second rows correspond to the dynamics of the one depicted in the first and second rows of Fig. 1, respectively (*i.e.*, for $\sigma = 30$ and $\sigma = 20.1$).

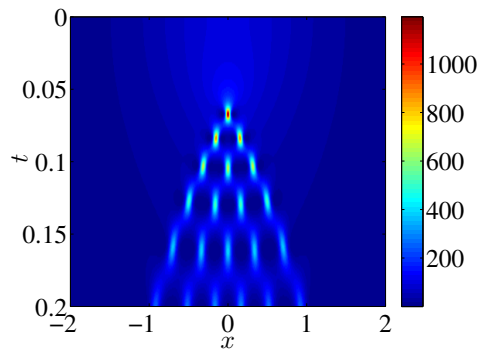


Fig. 3 – (Color online) Spatiotemporal evolution of the density $|u|^2$ based on initial data of the form of $u(x, t = 0) = 10 \operatorname{sech} x$.

π phase-jump for Peregrine solitons as well as the discussion in Ref. [94]). In any case, we should bear in mind that the extreme event observed in the respective cases of Fig. 1 is not a “genuine” Peregrine, but admittedly a coherent structure that very strongly resembles a Peregrine soliton near its core and also in its phase dynamics (see, Fig. 2). In fact, in this same core, it far more resembles (both in its decay and in its non-monotonicity and the structure of its side-blobs) to a Peregrine than to a best-fit soliton.

Furthermore, it should be noted that such representations tend to appear at earlier times as σ decreases (see, the accompanying movie [92]). However, an expanding structure, which we will refer to as a “Christmas tree” (CT) appears to emerge past the formation of the original (Peregrine-resembling) peak. As the structure expands, progressively at the peak emergence times more localized peaks arise (*i.e.*, we go from one to two, then to three, and so on). Such phenomenology has been first observed and extensively analyzed in Ref. [95], which is related to the umbilical gradient catastrophe therein. This work is closely related to the findings herein. Nevertheless, there are some nontrivial differences, including the fact that the analysis of Ref. [95] concerns patterns with a phase structure while our initial waveform is uniformly real. Perhaps more significantly, their analysis is limited to the semiclassical regime, which corresponds for our initial conditions to the case of large width σ . Nevertheless, in our numerical study, we perform a wide parametric continuation over values of σ . Moreover, below, we extend these considerations to the (apparently) non-integrable case of $\delta \neq 1$, which is not amenable to the analysis of Ref. [95]. That being said, we should comment that we expect that the “leaves” of the CT observed herein can be established in the appropriate limit pertinent to their methodology to be rational breathers of the NLS equation (NLSE). Moreover our results below can be thought of as a strong indication of the robustness of their findings even beyond the integrable case of $\delta = 1$.

A related remarkable (in our view) observation, however, is that in addition to the strong resemblance of the peak-structure in Fig. 1 with a Peregrine rogue wave (at the time of its peak, as well as in its appearance and disappearance), it is also strongly reminiscent of a multi-soliton pattern. In particular, we compare these profiles to N -soliton solutions [96] initialized at $t = 0$ as $u(x, t = 0) = N \operatorname{sech} x$; see also Refs. [97, 98] for a relevant discussion of this initial data in the integrable problem corresponding to $\delta = 1$.

To establish comparisons with the N -soliton solution as obtained from the inverse scattering method (see also the relevant clarification in the Introduction about the difference with the more colloquial wave form involving N individual *sech*-pulses), in Fig. 3 we show for reference, the case with $N = 10$; in addition, in Appendix 5, we provide the explicit analytical form and snapshots of the spatial profiles of the solitons for $N = 2$ and $N = 3$ (cf. left and right panels of Fig. 11, respectively).

It is relevant here to remind the reader that, generally, the initial condition $N \operatorname{sech} x$ leads to an N -soliton solution, as illustrated in Ref. [96]. Notably, the CT structure is clearly present in such a multi-soliton solution for N sufficiently large. Nevertheless, it is remarkable that the structure on the one hand has features strongly reminiscent of N -soliton initial conditions, yet at the same time it has this “centaurian” quality that its constituents are closely approximated by the algebraically decaying Peregrine wave structures.

We now turn to the case of smaller values of σ . In particular, numerical results corresponding to the cases with $\sigma = 5$, $\sigma = 3.1$, and $\sigma = 2.5$ are presented in the left, middle and right panels of Fig. 4, respectively. The respective number of solitons, N , predicted by Eq. (4) in these cases are $N = 4$ (for $\sigma = 5$) and $N = 2$ (for $\sigma = 3.1$ and $\sigma = 2.5$). It can be discerned from these panels that as the value of σ decreases, the N -soliton train (formed past the first high-peaked wave) starts decreasing in N , presumably going from a case associated with $N = 3$ (left panels) to ones with $N = 2$ in the middle and right panels. The latter two clearly feature the progression towards a time-periodic solution (see especially the $\sigma = 2.5$ case in the right panel). Yet, at the same time, in the spirit of centaurian qualities, this structure too can be very adequately approximated by the well-known Kuznetsov-Ma (KM) breather [18, 19].

A relevant fit of the center evolution to that of the center of a KM breather [85] (red circles based on the analytical expression) can be found in the bottom panel of the figure in the case of $\sigma = 2.5$. At the same time, as indicated above, the $N = 2$ solution features a similar-looking periodic dependence illustrated for comparison in Fig. 4(c). Thus, while we can clearly observe the progressively smaller number of solitons as σ decreases, both a 2-soliton structure and the KM breather bear characteristics closely resembling those of the solution for sufficiently small σ .

We now proceed to further decrease the value of σ , to values of about ≈ 1 . In this case, the high-peaked waveform emerging fits best into a (single) bright soliton described by Eq. (5) (in all previous examples depicted, the best fit of the core as indicated by the relevant snapshots was to a Peregrine). As an illustrative example, numerical results for the case of $\sigma = 1.3$ are shown in Fig. 5. Specifically, the right panel of the figure suggests a very good agreement between the numerically obtained solution and the exact one. As a side note, temporal oscillations of the density are observed, which are clearly demonstrated in the middle panel of the figure, *i.e.*, the pattern oscillates around a single bright soliton, given its Hamiltonian character, without relaxing fully to it.

Finally, we study the robustness of the reported numerical evolution results to perturbations in the initial data (induced, *e.g.*, by imperfections in the initial state preparation). To do so, we study the perturbation-induced dynamics of the NLSE (1) by adding a 50 dB (signal-to-noise ratio per sample) white noise to the localized region of the Gaussian pulse (3) specified by the full width at half maximum (FWHM);

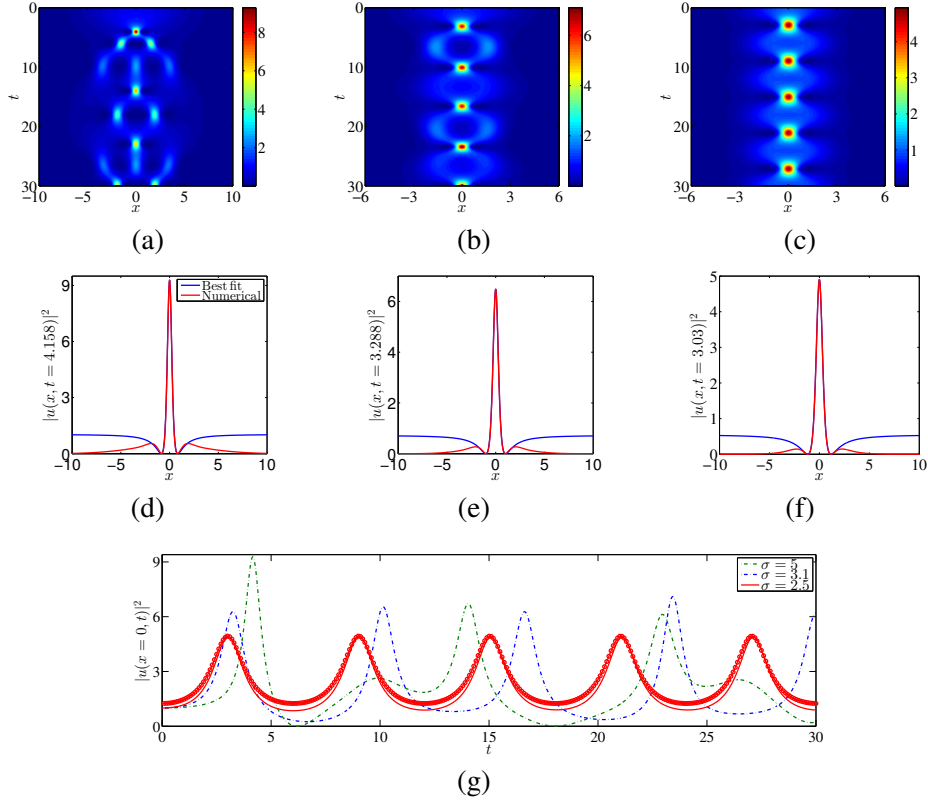


Fig. 4 – (Color online) *Top and middle rows*: Summary of results for $\sigma = 5$, $\sigma = 3.1$, and $\sigma = 2.5$ presented in left, middle, and right columns, respectively. Spatiotemporal evolution of densities $|u|^2$ (top row) as well as their spatial distribution (middle row) evaluated at $t = 4.158$, $t = 3.288$, and $t = 3.03$. Note that numerical and best-fit solutions are plotted against each other with solid red and blue lines, respectively, for comparison. *Bottom row*: Temporal evolution of the densities at $x = 0$ for various values of σ . Red circles correspond to best fit of the exact solution reported in [85].

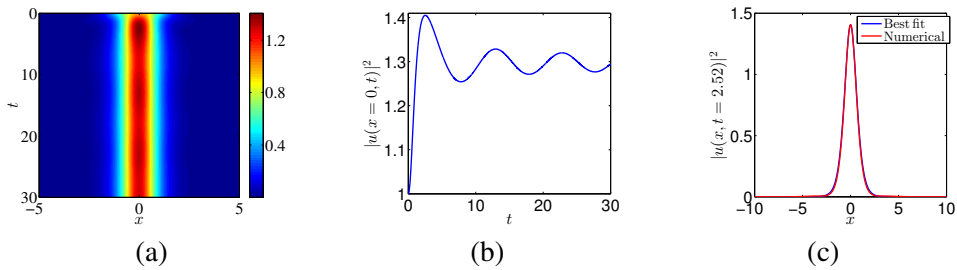


Fig. 5 – (Color online) Summary of results corresponding to $\sigma = 1.3$: The spatiotemporal evolution of the density $|u|^2$ is presented in the left panel. Case examples of the temporal and spatial distributions of the density are depicted in the middle and right panels, respectively. In the latter, a fit to a solitonic waveform is also presented (under “Best fit”).

see, also, Ref. [99] for a complete movie of the dynamics in this case. Highlights of our findings are shown in Fig. 6. The panel (a) of the figure showcases the evolution dynamics for $\sigma = 20.1$, to be compared with the unperturbed case of Fig. 1(d). Clearly, the results resembling the orderly CT structure (or the N -soliton solution that it may be representing) seem to lack persistence qualities in the present setting, as the resulting pattern clearly seems highly disordered, bearing little resemblance to its ordered origin. *Nevertheless*, its structural ingredients in the form of emergent peaks are still present and we have confirmed that they can still be well approximated (in fact, optimally approximated in comparison to single soliton) by Peregrine waveforms near the core. Hence, in some sense, the Peregrine-like features of the pattern appear to be robust. The above features were found to be manifested for a wide parametric window of σ values.

Nevertheless, as we gradually approach $\sigma \approx 10.5$, the dynamics are no longer affected dramatically by the perturbation. We report the case with $\sigma = 10.5$ in Fig. 6(b), where the formation of a rogue wave is followed by the previously mentioned expanding CT structure potentially attributable to an N -soliton solution. By decreasing the value of σ further, the noise does not affect the dynamics essentially at all. This is clearly illustrated in the cases featured in Fig. 6(c) and Fig. 6(d), where the apparent $N = 2$ and $N = 1$ solitons seem to clearly persist.

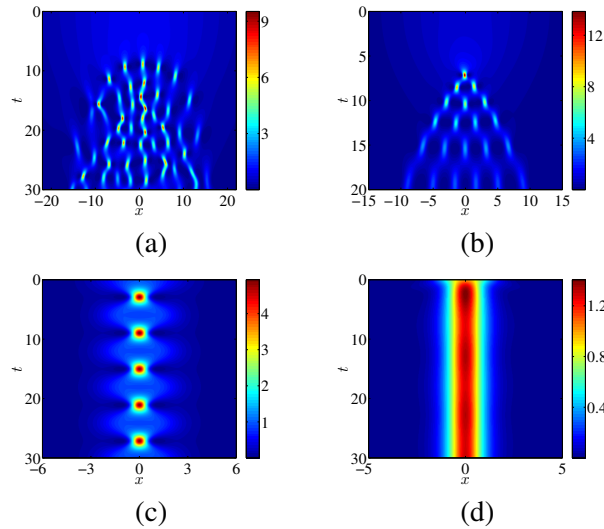


Fig. 6 – (Color online) Spatiotemporal evolution of the density $|u|^2$ corresponding to perturbed cases with (a) $\sigma = 20.1$, (b) $\sigma = 10.5$, (c) $\sigma = 2.5$, and (d) $\sigma = 1.3$. The first one appears to destroy the CT structure, while the second one to preserve it. In (c) and (d), the patterns closely resemble the $N = 2$ and $N = 1$ soliton states. For the former solution, see panel (c) of Fig. 11 in the Appendix 5.

3.2. THE NONINTEGRABLE CASE: $\delta > 1$

Having studied the integrable case, we now turn to the nonintegrable one corresponding to $\delta > 1$. We are interested in identifying parametric case examples of σ and δ for which collapsing events may take place and, perhaps more importantly, understanding the underlying mechanisms that are responsible for creating such eventual evolutionary phenomena. That is, as δ is increased beyond the quintic term of $\delta = 2$, the focusing becomes amenable to wave collapse [80] through the bifurcation of self-similar waveforms [100]. It is then intriguing to explore to what degree the possibility of extreme events, like Peregrine solitons, may interplay with the self-similar structures in producing such collapse events.

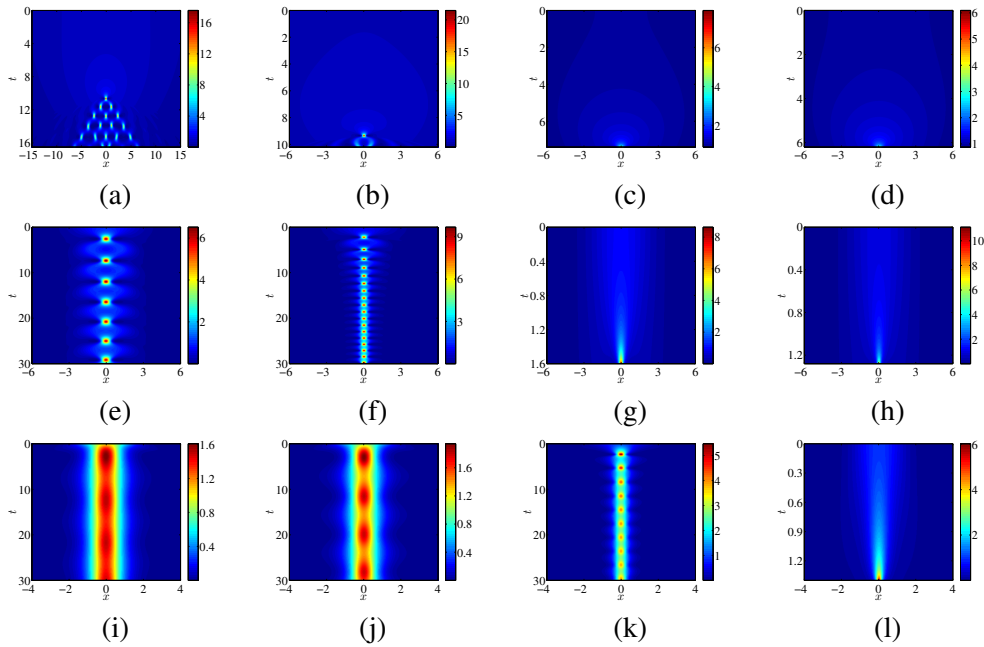


Fig. 7 – (Color online) Spatiotemporal evolution of the density $|u|^2$ corresponding to the nonintegrable NLS equation with (a)-(d) $\sigma = 20.1$, (e)-(h) $\sigma = 2.5$ and (i)-(l) $\sigma = 1.3$. First, second, third, and fourth columns correspond to values of nonlinearity power of $\delta = 1.2$, $\delta = 1.4$, $\delta = 1.8$ and $\delta = 2.2$, respectively. A detailed interpretation of these observations is given in the text.

Here, it should be pointed out that the solutions given by Eqs. (5) and (6) cannot be used in the subsequent analysis, due to the fact that neither constitutes a solution to the NLS equation for $\delta > 1$. On the other hand, the soliton solution can be generalized

in this setting, taking the form

$$u(x, t) = \left(\frac{A}{2}\right)^{\frac{1}{2\delta}} \left[\operatorname{sech} \left(\delta \sqrt{\frac{A}{\delta+1}} (x - x_0) \right) \right]^{\frac{1}{\delta}} \exp(i\beta t), \quad (11)$$

with $\beta = A/[2(1 + \delta)]$. This fact naturally raises the interesting question of whether Peregrine waveforms may also generalize in this setting. This is a question particularly interesting in its own right, which, to the best of our knowledge, has not been addressed as of yet.

To present a broad perspective of the corresponding interplay, we showcase numerical results for different values of the nonlinearity power δ by employing the same Gaussian initial data (3), also varying the width σ (for fixed amplitude, $\alpha = 1$); this is a map, presented in Fig. 7, of the two parameter space of the system and its corresponding dynamical response. Specifically, we present results with $\sigma = 20.1$ (that is, within the interval of σ where the CT structure previously emerged), $\sigma = 2.5$ (where a breathing pattern reminiscent of both the KM breather and the $N = 2$ soliton arose) and $\sigma = 1.3$ (the fundamental soliton regime) in Fig. 7 for different values of δ . See, also, Refs. [101] for complete movies of the dynamics corresponding to example cases with $\delta = 1.2$, $\delta = 1.4$ as well as $\delta = 2.2$, together with their perturbed versions in Refs. [102]. It should be stressed that the final times showed in Fig. 7 have been selected in a way such that our numerical scheme is still expected to properly capture the dynamics. That is to say, when the solution of the IVP presented focusing events such that the width of the solution became comparable to the (selected to be very small) grid spacing, the simulation was stopped before the occurrence of such an event. While, admittedly, techniques based on adaptive mesh refinement and dynamic rescaling exist [103] (see, also, [104]) may allow to continue these events further; for the purposes of this study, we consider these events to be faithful precursors of very strong focusing (conducive to collapse or in any event regimes where the NLS model would no longer be applicable in physical settings and higher-order terms would come into play).

We can see in the top row of Fig. 7, corresponding to $\sigma = 20.1$ (see also, for comparison, the bottom row of Fig. 1), that as we progressively increase the value of δ , the formation of the CT structure is persistent in panel (a) for $\delta = 1.2$, while panel (b) for $\delta = 1.4$ also supports a peak reminiscent of the extreme events discussed previously, that can be mapped adequately by a local core fit to a Peregrine structure. However, in panels (c) and (d) (for $\delta = 1.8$ and $\delta = 2.2$, respectively) the evolution of the density leads to strong focusing events as discussed previously although, importantly, in the former case we are not in the regime (of $\delta \geq 2$) where regular solitons become unstable towards collapse; notice nevertheless the structural similarity of these two events. This suggests that, in some way, the formation of these extreme

events may promote strong focusing even in cases where the self-similar collapsing solutions (and the instability of regular solitons) are not supported, *i.e.*, these events may be *triggered* by the Peregrine-like entities observed herein. To further enhance this perspective, the middle row of the figure showcases results for $\sigma = 2.5$ corresponding to the breathing solution (of considerably smaller number of atoms/squared L^2 norm).

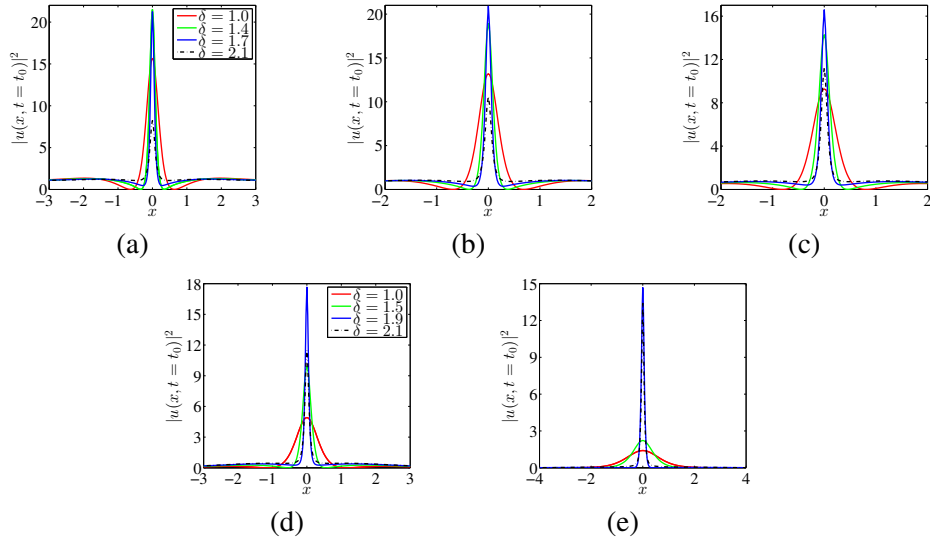


Fig. 8 – (Color online) Snapshots of the densities $|u|^2$ at $t = t_0$ (see, text for details) and for various values of δ (see legends) and σ . Panels (a), (b), and (c) correspond to $\sigma = 20.1$, 10.5 , and 5 , whereas panels (d) and (e) to $\sigma = 2.5$ and 1.3 , respectively.

The density, through its deformation (see panel (e)) for $\delta = 1.2$, starts becoming more localized in the middle of the spatial grid, *i.e.*, at $x = 0$ (see, panel (f) corresponding to $\delta = 1.4$ therein) with a rapidly decreasing vibration period, until the dynamics leads again to strong focusing (see panels (g) and (h) of the figure). Yet, once again in (g), we are below the threshold of $\delta = 2$. Finally, and as per the soliton regime (see Fig. 5 corresponding to $\sigma = 1.3$, for comparison), the bottom panels reveal that the fundamental soliton progressively becomes localized at $x = 0$ as δ increases until it collapses for $\sigma = 2.2$. In this case, collapse-resembling features are not apparent, except for the supercritical case of $\delta = 2.2$.

We have used different types of diagnostics in order to capture the trends of the variation over σ and δ . We have found, for instance, that the times t_0 associated with the appearance of the first peak structure typically decrease (with a notable exception within the so-called soliton regime of very small σ) as δ is increased, *i.e.*,

the effect of δ increasing clearly promotes focusing. The strength of the focusing (the intensity of the peak event) is more substantial too when δ is increased or when σ (and the overall power) is decreased (data not shown). However, as an additional diagnostic here, snapshots of densities for various values of σ are shown in Fig. 8 with the aim to shed some light on the nature of the structures that trigger the high intensity events. It can be discerned from these plots that the formation of a high-amplitude wave surrounded by two minima corresponding to zeros of the density is evident for $\delta = 1$ (denoted by solid red lines in the figure) and for all the cases with $\sigma > 1.3$. Such localized structures are reminiscent of the Peregrine soliton, although for larger δ (> 1) the locations of the minima are approaching to each other and no longer correspond to zeros of the density (see how the relevant spatial distribution has been lifted up). Thus, our results suggest that the Peregrine-like pattern emerging (and rapidly disappearing) in the dynamics is crucially responsible for the strong focusing featured by this generalized NLS dynamics even for $\delta < 2$. Progressively as δ approaches (and especially surpasses) 2, and even more so as σ decreases (where the pattern resembles more a regular soliton), we encounter the familiar bell-shaped collapse. This numerical evidence suggests that the potential existence of rogue-like structures may promote large amplitude dynamics resembling collapse even below the critical point of the (generalized) NLS model.

4. SIMILARITIES AND DIFFERENCES BETWEEN THE NPSE AND THE 3D GPE

Our aim in this Section is to briefly illustrate some of the similarities, as well as differences between the more standard NLS and generalized NLS models of the previous Section and the results of the more accurate, in the context of atomic condensates, 1D NPSE and 3D GPE. The two equations were generally found to provide similar results qualitatively, hence, we only present selected case examples from each one. In order to analyze the outcome from the initial condition (3), we have taken several values of σ . Collapse takes place as long as the amplitude α is larger than a critical value that differs between the cases of $\Omega = 0$ and $\Omega \neq 0$. We have considered the dynamics for α slightly below the critical one to again showcase the phenomenology as large amplitude extreme events are approached.

A prototypical example of our results for the NPSE model is provided in Fig. 9. Here, the value of σ chosen was 20, although we also performed similar runs for $\sigma = 10$ and $\sigma = 5$ without obtaining dramatically different results. What can be seen for different amplitudes in the figure is that the solution has a clearly breathing character (this is especially evident in the bottom panels), with large focusing events similar to the events we classified in the previous Section. That being said, much of the recurrence phenomenology in this case is lost – except if the trap induces

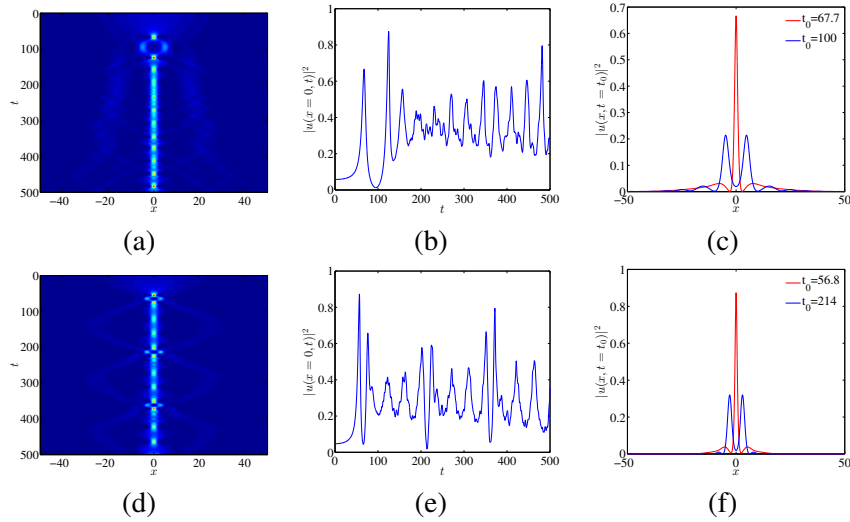


Fig. 9 – Summary of results corresponding to the NPSE for $\sigma = 20$ with $\alpha = 0.2405$ and $\Omega = 0$ (top row) and $\alpha = 0.2172$ and $\Omega = \Omega_0$ (bottom row). The respective spatiotemporal evolution of the density $|u|^2$ is presented in panels (a) and (d). The global maximum of the density $|u(x = 0, t)|^2$ as a function of time t is shown in panels (b) and (e). Density profile at times t_0 (when the first maximum is observed as well as at later times when the maximum separation between the humps is attained) of panels (b) and (e) is shown in panels (c) and (f), respectively.

it, as seems to be partially the case in the bottom panel. Even more importantly prototypical structures that much of our analysis of the previous Section was based on – such as the CT waveform – are completely absent, suggesting that the strong non-integrability of the NPSE model is partially detrimental to such features.

To corroborate that these types of features also appear in the 3D GPE, we have selected a prototypical example of the latter as well, shown in Fig. 10. Here, we observe that again despite the relatively large value of σ , only a beating oscillation is observed, *i.e.*, there is no evidence of the CT structure. Nevertheless, the formation of the peak again seems to have structural characteristics [through its brief appearance and subsequent disappearance (top left and top right panels), the formation of the (vanishing density in the bottom left panel) local minima etc.] of Peregrine-like patterns rather than of permanent solitonic ones. At the same time, though, in the precursors to large density focusing in this case, features of significant transverse excitation are amply evident, *e.g.*, in the bottom right panel, hence here the role of higher dimensionality is also important towards appreciating the full dynamical evolution.

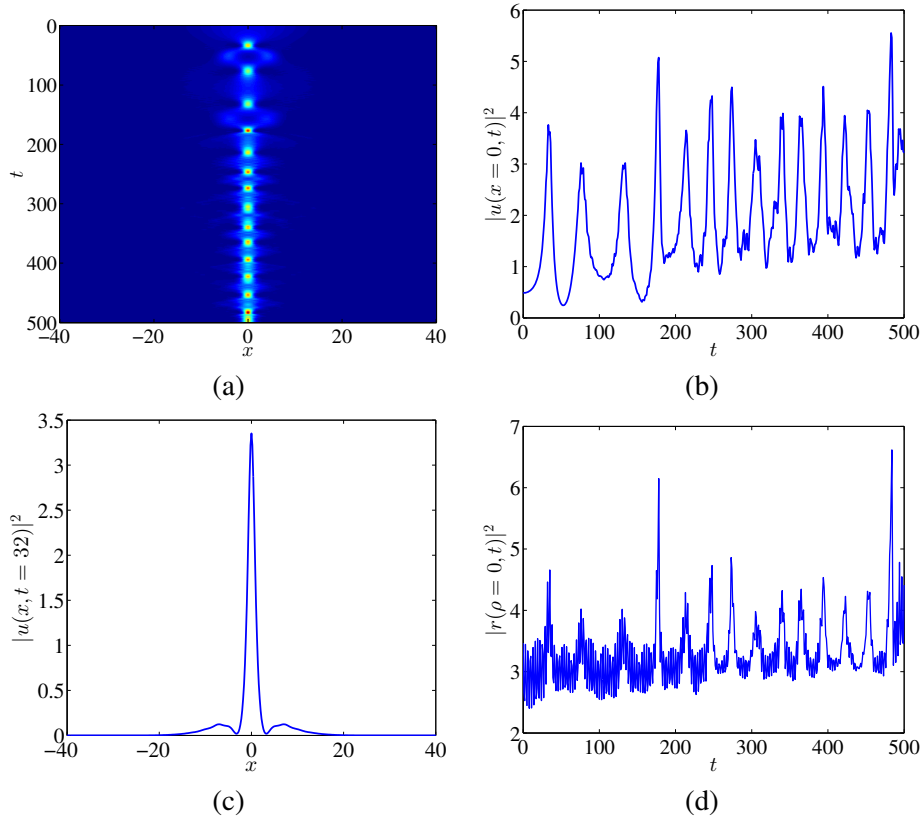


Fig. 10 – Summary of results corresponding to the 3D GPE for $\sigma = 10$ and $\alpha = 0.6697$ (just below the collapse threshold). (a) Spatiotemporal evolution of the longitudinal excitations density $|u|^2$, with $u(x,t) = 2\pi \int_0^\infty \rho d\rho |\psi(\rho, x, t)|^2$. (b) The global maximum of the longitudinal excitations density $|u(x=0,t)|^2$ as a function of time t . (c) Density profile associated with panel (b) at $t = 32$, *i.e.*, when the first maximum is observed. (d) The global maximum of the transverse excitations density $|r|^2$, with $r(\rho, t) = \int_{-\infty}^{+\infty} dx |\psi(\rho, x, t)|^2$, evaluated at $\rho = 0$ as a function of time t for the 3D equation.

5. CONCLUSIONS AND FUTURE CHALLENGES

The intention of this work was, to a large extent, to raise intriguing questions and perhaps to a smaller degree, to provide partial answers. One question was/is: are there initial data whose evolution will resemble an extreme event (and perhaps more concretely a Peregrine soliton) in NLS systems ? The answer seems to generally be yes, in fact, even stemming from rather generic initial data, such as a Gaussian. The NLS model itself and “mild” variations thereof (such as the generalized power model, for exponents close to the cubic case) seem to in fact bear more complex features, such as the “Christmas tree” structure that we observed and whose phenomenology appears to be intimately related to the umbilical gradient catastrophe in the terminology of Ref. [95]. Another question was/is: do these rogue-wave-like patterns have a role in collapse-type phenomena ? Again, we believe that numerical simulations seem to be strongly suggestive in that direction, in fact promoting such phenomena for models that do not feature self-similarly collapsing solutions (such as the generalized NLS model with nonlinearities of exponent below the critical quintic case). Do these features appear to persist in applications including three-dimensional systems inspired by the physics of atomic condensates ? Our numerical experiments here suggest that this is only partially the case – *i.e.*, Peregrine-like waveforms may seem persistent but other features such as the “Christmas tree” patterns are definitely absent in the latter setting.

On the other hand, there are many more questions that are either not answered or that are perhaps created by these results. For example, we cannot distinguish definitively if the patterns that emerge resemble more arrays of Peregrine solitons or whether they are more N -soliton like solutions for N large; what is the connection between the two ? Similarly, questions involving understanding a potential connection between structures like the 2-soliton and Kuznetsov-Ma breather also arise. Characterizing the outcome of the inverse scattering problem for the NLS (Zakharov-Shabat) for a prototypical Gaussian initial state naturally emerges as an important problem to solve. Another question for theoretical consideration is whether there is an explicit analogue of the Peregrine soliton for the case of the generalized NLS model with the exponent δ . We argued that the Peregrine-like patterns seem responsible for the enhanced focusing, but could one “distinguish” the contributing role of a Peregrine and that of a soliton in inducing collapse phenomena ? Also, do collapse events mathematically truly arise for $\delta < 2$? Of course, the over-arching (and perhaps over-shadowing) query is: would it be possible to observe experimentally rogue waves in such ultracold bosonic seas ? These questions suggest an intriguing array of investigations lying ahead.

APPENDIX: EXPLICIT FORM OF $N = 2$ AND $N = 3$ SOLITON SOLUTIONS

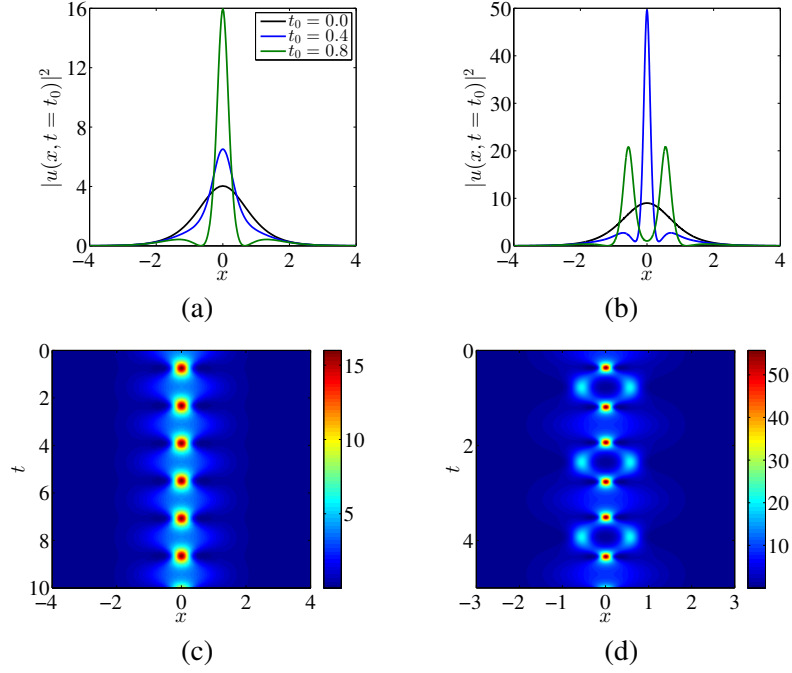


Fig. 11 – (Color online) Numerical examples of $N = 2$ and $N = 3$ soliton solutions depicted in the left and right columns, respectively. Specifically, the top row panels correspond to spatial distributions of the density $|u|^2$ at $t = t_0$ (see, the legend therein) for the respective cases whereas the bottom row panels showcase its spatiotemporal evolution.

In this Appendix, we briefly discuss the explicit form of the $N = 2$ and $N = 3$ soliton solutions (denoted by $u_{2s}(x, t)$ and $u_{3s}(x, t)$, respectively) to the integrable NLSE (1). In particular, they are given by

$$u_{2s}(x, t) = 4 \frac{\cosh(3x) + 3 \exp(4it) \cosh x}{3 \cos(4t) + 4 \cosh(2x) + \cosh(4x)} \exp(it/2), \quad (12)$$

and

$$u_{3s}(x, t) = 3 \frac{G(x, t)}{F(x, t)} \exp(it/2), \quad (13)$$

respectively, where

$$\begin{aligned}
 G(x, t) &= 45 \exp(8it) + 5 \exp(-8it) + 20 \exp(16it) + 32 \cosh(2x) + 2 \cosh(8x) \\
 &\quad + [80 \cosh(2x) + 20 \cosh(4x)] \exp(12it) \\
 &\quad + [36 \cosh(4x) + 16 \cosh(6x)] \exp(4it), \\
 F(x, t) &= 90 \cos(8t) \cosh x + 20 \cos(12t) \cosh(3x) + 36 \cos(4t) \cosh(5x) \\
 &\quad + 36 \cosh x + 64 \cosh(3x) + 9 \cosh(7x) + \cosh(9x).
 \end{aligned} \tag{14}$$

For further details, see [96] and [105].

Indicatively, we demonstrate numerical results for the $N = 2$ (left column) and $N = 3$ (right column) soliton solutions in Fig. 11. In particular, we initialize the dynamics of NLSE (1) at $t = 0$ using Eqs. (12) and (13) for the respective cases and evolve the latter forward in time while monitoring the dynamical evolution of the density $|u|^2$. It should be pointed out that both Eqs. (12) and (13) evaluated at $t = 0$ result in $N \operatorname{sech} x$ as expected, of course.

Acknowledgements. J.C.-M. thanks financial support from the project MAT2016-79866-R (AEI/FEDER, UE). P.G.K. and D.J.F. acknowledge that this paper was made possible by NPRP grant # [8 – 764 – 1 – 160] from the Qatar National Research Fund (a member of Qatar Foundation). The findings achieved herein are solely the responsibility of the authors. E.G.C. thanks Theodoros Horikis (University of Ioannina) for providing help in connection with the spectral code for the NLS equation as well as Dionyssios Mantzavinos (UMass) for constructive discussions about the N -soliton solutions. P.G.K. and D.J.F. also thank Theodoros Horikis for multiple fruitful discussions at the beginning of this project. P.G.K. also thanks Gino Biondini (SUNY Buffalo), Themistoklis Sapsis (MIT), and Andrei Ludu (Embry-Riddle Aeronautical University) for discussions. P.G.K. acknowledges support from the National Science Foundation under Grant DMS-1312856 and from FP7-People under Grant No. IRSES-605096.

REFERENCES

1. E. Pelinovsky and C. Kharif (eds.), *Extreme Ocean Waves*, Springer, NY, 2008.
2. C. Kharif, E. Pelinovsky, and A. Slunyaev, *Rogue Waves in the Ocean*, Springer, NY, 2009.
3. A. R. Osborne, *Nonlinear Ocean Waves and the Inverse Scattering Transform*, Academic Press, Amsterdam, 2010.
4. D. R. Solli, C. Ropers, P. Koonath, and B. Jalali, *Nature* **450**, 1054 (2007).
5. B. Kibler *et al.*, *Nature Phys.* **6**, 790 (2010).
6. B. Kibler *et al.*, *Sci. Rep.* **2**, 463 (2012).
7. J. M. Dudley, F. Dias, M. Erkintalo, and G. Genty, *Nat. Photon.* **8**, 755 (2014).
8. B. Frisquet *et al.*, *Sci. Rep.* **6**, 20785 (2016).
9. C. Lecaplain, Ph. Grelu, J. M. Soto-Crespo, and N. Akhmediev, *Phys. Rev. Lett.* **108**, 233901 (2012).
10. A. N. Ganshin, V. B. Efimov, G. V. Kolmakov, L. P. Mezhov-Deglin, and P. V. E. McClintock, *Phys. Rev. Lett.* **101**, 065303 (2008).
11. A. Chabchoub, N. P. Hoffmann, and N. Akhmediev, *Phys. Rev. Lett.* **106**, 204502 (2011).

12. A. Chabchoub, N. Hoffmann, M. Onorato, and N. Akhmediev, *Phys. Rev. X* **2**, 011015 (2012).
13. A. Chabchoub and M. Fink, *Phys. Rev. Lett.* **112**, 124101 (2014).
14. H. Xia, T. Maimbourg, H. Punzmann, and M. Shats, *Phys. Rev. Lett.* **109**, 114502 (2012).
15. M. Shats, H. Punzmann, and H. Xia, *Phys. Rev. Lett.* **104**, 104503 (2010).
16. H. Bailung, S. K. Sharma, and Y. Nakamura, *Phys. Rev. Lett.* **107**, 255005 (2011).
17. D. H. Peregrine, *J. Austral. Math. Soc. B* **25**, 16 (1983).
18. E. A. Kuznetsov, *Sov. Phys.-Dokl.* **22**, 507 (1977).
19. Ya. C. Ma, *Stud. Appl. Math.* **60**, 43 (1979).
20. N. N. Akhmediev, V. M. Eleonskii, and N. E. Kulagin, *Theor. Math. Phys.* **72**, 809 (1987).
21. K. B. Dysthe and K. Trulsen, *Phys. Scr.* **T82**, 48 (1999).
22. Z. Yan, *J. Phys. Conf. Ser.* **400**, 012084 (2012).
23. P. T. S. DeVore, D. R. Solli, D. Borlaug, C. Ropers, and B. Jalali, *J. Opt.* **15**, 0640031 (2013).
24. M. Onorato, S. Residori, U. Bortolozzo, A. Montina, and F. T. Arecchi, *Phys. Rep.* **528**, 47 (2013).
25. D. Mihalache, *Rom. Rep. Phys.* **69**, 403 (2017).
26. C. J. Pethick and H. Smith, *Bose-Einstein Condensation in Dilute Gases*, Cambridge University Press, Cambridge, 2008.
27. L. P. Pitaevskii and S. Stringari, *Bose-Einstein Condensation*, Oxford University Press, Oxford, 2003.
28. V. S. Bagnato, D. J. Frantzeskakis, P. G. Kevrekidis, B. A. Malomed, and D. Mihalache, *Rom. Rep. Phys.* **67**, 5 (2015).
29. P. G. Kevrekidis, D. J. Frantzeskakis, and R. Carretero-González (eds.), *Emergent Nonlinear Phenomena in Bose-Einstein Condensates. Theory and Experiment*, Springer-Verlag, Berlin, 2008; R. Carretero-González, D. J. Frantzeskakis, and P. G. Kevrekidis, *Nonlinearity* **21**, R139 (2008).
30. P. G. Kevrekidis, D. J. Frantzeskakis, and R. Carretero-González, *The defocusing Nonlinear Schrödinger Equation: From Dark Solitons to Vortices and Vortex Rings*, SIAM, Philadelphia, 2015.
31. I. Carusotto and C. Ciuti, *Rev. Mod. Phys.* **85**, 299 (2013).
32. K. E. Strecker, G. B. Partridge, A. G. Truscott, and R. G. Hulet, *Nature* **417**, 150 (2002).
33. L. Khaykovich, F. Schreck, G. Ferrari, T. Bourdel, J. Cubizolles, L. D. Carr, Y. Castin, and C. Salomon, *Science* **296**, 1290 (2002).
34. S. L. Cornish, S. T. Thompson, and C. E. Wieman, *Phys. Rev. Lett.* **96**, 170401 (2006).
35. O. Morsch and M. Oberthaler, *Rev. Mod. Phys.* **78**, 179 (2006).
36. D. J. Frantzeskakis, *J. Phys. A* **43**, 213001 (2010).
37. P. Engels, C. Atherton, and M. A. Hofer, *Phys. Rev. Lett.* **98**, 095301 (2007).
38. A. I. Nicolin, R. Carretero-González, and P. G. Kevrekidis, *Phys. Rev. A* **76**, 063609 (2007).
39. A. I. Nicolin, *Phys. Rev. E* **84**, 056202 (2011).
40. A. Balaž and A. I. Nicolin, *Phys. Rev. A* **85**, 023613 (2012).
41. A. Balaž, R. Paun, A. I. Nicolin, S. Balasubramanian, and R. Ramaswamy, *Phys. Rev. A* **89**, 023609 (2014).
42. J. B. Sudharsan, R. Radha, M. C. Raportaru, A. I. Nicolin, and A. Balaž, *J. Phys. B-At. Mol. Opt. Phys.* **49**, 165303 (2016).
43. A. L. Fetter and A. A. Svidzinsky, *J. Phys.: Cond. Mat.* **13**, R135 (2001).
44. A. L. Fetter, *Rev. Mod. Phys.* **81**, 647 (2009).
45. S. Komineas, *Eur. Phys. J.- Spec. Topics* **147**, 133 (2007).
46. Yu. V. Bludov, V. V. Konotop, and N. Akhmediev, *Phys. Rev. A* **80**, 033610 (2009).
47. S. Rajendran, P. Muruganandam, and M. Lakshmanan, *Physica D* **239**, 366 (2010).

48. Z. Yan, Phys. Lett. A **374**, 672 (2010).
49. L. Wen, L. Li, Z. D. Li, S. W. Song, X. F. Zhang, and W. M. Liu, Eur. Phys. J. D **64**, 473 (2011).
50. L.-C. Zhao, Annals of Phys. **329**, 73 (2013).
51. J. S. He, E. G. Charalampidis, P. G. Kevrekidis, and D. J. Frantzeskakis, Phys. Lett. A **378**, 577 (2014).
52. S. Loomba, H. Kaur, R. Gupta, C. N. Kumar, and T. S. Raju, Phys. Rev. E **89**, 052915 (2014).
53. K. Manikandan, P. Muruganandam, M. Senthilvelan, and M. Lakshmanan, Phys. Rev. E **90**, 062905 (2014).
54. S. Rajendran, P. Muruganandam, and M. Lakshmanan, J. Phys. B: At. Mol. Opt. Phys. **42**, 145307 (2009).
55. Yu. V. Bludov, V. V. Konotop, and N. Akhmediev, Eur. Phys. J. Spec. Top. **185**, 169 (2010).
56. F. Baronio, A. Degasperis, M. Conforti, and S. Wabnitz, Phys. Rev. Lett. **109**, 044102 (2012).
57. P. S. Vinayagam, R. Radha, and K. Porsezian, Phys. Rev. E **88**, 042906 (2013).
58. R. Babu Mareeswaran, E. G. Charalampidis, T. Kanna, P. G. Kevrekidis, and D. J. Frantzeskakis, Phys. Rev. E **90**, 042912 (2014).
59. W.-P. Zhong, M. Belić, and B. A. Malomed, Phys. Rev. E **92**, 053201 (2015).
60. K. Manikandan, P. Muruganandam, M. Senthilvelan, and M. Lakshmanan, Phys. Rev. E **93**, 032212 (2016).
61. R. Babu Mareeswaran and T. Kanna, Phys. Lett. A **380**, 3244 (2016).
62. Z. Qin and G. Mu, Phys. Rev. E **86**, 036601 (2012).
63. L.-C. Zhao and J. Liu, Phys. Rev. E **87**, 013201 (2013).
64. Y.-J. Shen, Y. -T. Gao, D.-W. Zuo, Y. -H. Sun, Y. -J. Feng, and L. Xue, Phys. Rev. E **89**, 062915 (2014).
65. K. Manikandan, M. Senthilvelan, and R. A. Kraenkel, Eur. Phys. J. B **89**, 30 (2016).
66. Z. Yan, V. V. Konotop, and N. Akhmediev, Phys. Rev. E **82**, 036610 (2010).
67. K. Henderson, C. Ryu, C. MacCormick, and M. G. Boshier, New J. Phys., **11**, 043030 (2009).
68. J. H. V. Nguyen, D. Luo, R. G. Hulet, Science, **356**, 422 (2017).
69. N. Akhmediev, A. Ankiewicz, and M. Taki, Phys. Lett. A **373**, 675 (2009).
70. N. Akhmediev, J. M. Soto-Crespo, and A. Ankiewicz, Phys. Lett. A **373**, 2137 (2009).
71. V. E. Zakharov, A. I. Dyachenko, and A. O. Prokofiev, Eur. J. of Mech. B/Fluids **25**, 677 (2006).
72. G. Biondini and D. Mantzavinos, Phys. Rev. Lett. **116**, 043902 (2016).
73. L. Salasnich, A. Parola, and L. Reatto, Phys. Rev. A **65**, 043614 (2002).
74. A. Weller *et al.*, Phys. Rev. Lett. **101**, 130401 (2008).
75. S. Middelkamp *et al.*, Phys. Lett. A **375**, 642 (2011).
76. J. Cuevas, P. G. Kevrekidis, B. A. Malomed, P. Dyke, and R. G. Hulet, New J. Phys., **15**, 063006 (2013).
77. R. Kanamoto, L. D. Carr, and M. Ueda, Phys. Rev. Lett. **100**, 060401 (2008);
R. Kanamoto, L. D. Carr, and M. Ueda, Phys. Rev. A **79**, 063616 (2009).
78. M. Syafwan, P. Kevrekidis, A. Paris-Mandoki, I. Lesanovsky, P. Kruger, L. Hackermuller, and H. Susanto, J. Phys. B: At. Mol. Opt. Phys. **49**, 235301 (2016).
79. N. G. Parker, A. M. Martin, C. S. Adams, and S. L. Cornish, Physica D **238**, 1456 (2009).
80. C. Sulem and P. L. Sulem, *The Nonlinear Schrödinger Equation*, Springer-Verlag, New York, 1999.
81. Contrary to the NLSE given by Eq. (1), the model (2) results in collapse dynamics when $|u|^2 \rightarrow 1$, that is, when the density of the field u becomes sufficiently close to unity. Thus, this limit imposes an upper bound on the amplitude of the initial condition employed [see Eq. (3)]. However, it should

- be noted in passing that this limitation will be bypassed when we consider the full 3D model from which the NPSE originates from (see, the corresponding discussion below).
82. M. J. Ablowitz, B. Prinari, and A. D. Trubatch, *Discrete and Continuous Nonlinear Schrödinger Systems*, Cambridge University Press, Cambridge, 2004.
 83. M. Klaus and J. K. Shaw, *Phys. Rev. E* **65**, 036607 (2002).
 84. M. Klaus and J. K. Shaw, *SIAM J. Appl. Math.* **34**, 759 (2003).
 85. K. Hammami, B. Kibler, C. Finot, P. Morin, J. Fatome, J. M. Dudley, and G. Millot, *Opt. Lett.* **36**, 112 (2011).
 86. A.-K. Kassam and L. N. Trefethen, Fourth-order time stepping for stiff PDEs, *SIAM J. Sci. Comp.* **26**, 1214 (2005).
 87. P. Muruganandam and S. K. Adhikari, *Comput. Phys. Commun.* **180**, 1888 (2009).
 88. D. Vudragović, I. Vidanović, A. Balaž, P. Muruganandamm, and S. K. Adhikari, *Comput. Phys. Commun.* **183**, 2021 (2012).
 89. R. K. Kumar, L. E. Young-S., D. Vudragović, A. Balaž, P. Muruganandamm, and S. K. Adhikari, *Comput. Phys. Commun.* **195**, 117 (2015).
 90. V. Lončar, A. Balaž, A. Bogojević, S. Škrbić, P. Muruganandam, and S. K. Adhikari, *Comput. Phys. Commun.* **200**, 406 (2016).
 91. V. Lončar, L. E. Young-S., S. Škrbić, P. Muruganandam, S. K. Adhikari, and A. Balaž, *Comput. Phys. Commun.* **209**, 190 (2016).
 92. <https://youtu.be/LzRj7dGzOtY>
 93. T. P. Horikis and M. J. Ablowitz, *Phys. Rev. E* **95**, 042211 (2017).
 94. A. Tikan, C. Billet, G. El, A. Tovbis, M. Bertola, T. Sylvestre, F. Gustave, S. Randoux, G. Genty, P. Suret, and J. M. Dudley, *arXiv:1701.08527*
 95. M. Bertola and A. Tovbis, *Comm. Pure Appl. Math.* **66**, 678 (2013).
 96. J. Satsuma and N. Yajima, *Prog. Theor. Phys. Supplement* **55**, 284 (1974).
 97. L. Lee, G. Lyng, and I. Vankova, *Phys. D* **241**, 1767 (2012).
 98. Y. Kim, L. Lee, and G. Lyng, *J. Math. Phys.* **55**, 083516 (2014).
 99. <https://youtu.be/h4c2057ePtw>
 100. C. I. Siettos, I. G. Kevrekidis, and P. G. Kevrekidis, *Nonlinearity* **16**, 497 (2003).
 101. <https://youtu.be/UDM7TVe1-jQ> ($\delta = 1.2$);
<https://youtu.be/lci-E835P8E> ($\delta = 1.4$);
<https://youtu.be/ONUPWcSnCBQ> ($\delta = 2.2$).
 102. <https://youtu.be/TfOZ1tYUaf4> ($\delta = 1.2$);
<https://youtu.be/rfCWHJwNkYU> ($\delta = 1.4$);
<https://youtu.be/1TclP5tDa4g> ($\delta = 2.2$).
 103. W. Ren and X. P. Wang, *J. Comp. Phys* **159**, 246 (2000).
 104. W. Huang and R. D. Russell, *Adaptive Moving Mesh Methods*, Springer, 2011.
 105. A. I. Maimistov and A. M. Basharov, *Nonlinear Optical Waves*, Springer Netherlands, 1999.